The European Large Area ISO Survey – IX. The 90-μm luminosity function from the Final Analysis sample

Stephen Serjeant,[1]⋆† Alberto Carramiñana,[2]† Eduardo Gonzáles-Solares,[14]
Phillipe Héraudeau,[4,5] Raúl Mújica,[2]† Ismael Perez-Fournon,[6] Nicola Sedgwick,[1]†
Michael Rowan-Robinson,[7] Alberto Franceschini,[9] Thomas Babbedge,[7]
Carlos del Burgo,[13] Paolo Ciliegi,[8] Andreas Efstathiou,[12] Fabio La Franca,[10]
Carlotta Gruppioni,[8] David Hughes,[2] Carlo Lari,[11] Seb Oliver,[3]
Francesca Pozzi,[11] Manfred Stickel[5] and Mattia Vaccari[9]

[1]*Centre for Astrophysics & Planetary Science, School of Physical Sciences, University of Kent, Canterbury, Kent CT2 7NR*
[2]*Instituto Nacional de Astrofísica, Óptica y Electrónica, Luis Enrique Erro 1, Tonantzintla, Puebla 72840, Mexico*
[3]*Astronomy Centre, CPES, University of Sussex, Falmer, Brighton BN1 9QJ*
[4]*Kapteyn Astronomical Institute, Postbus 800, 9700 AV Groningen, the Netherlands*
[5]*Max-Planck-Institut für Astronomie, Köningstuhl 17, D-69117, Heidelberg, Germany*
[6]*Instituto de Astrofisica de Canarias, C/Vía Láctea s/n. 38200 La Laguna, Tenerife, Spain*
[7]*Astrophysics Group, Imperial College London, Blackett Laboratory, Prince Consort Road, London SW7 2BW*
[8]*Bologna Astronomical Observatory, Via Ranzani 1, 40127 Bologna, Italy*
[9]*Dipartimento di Astronomia, Università di Padova, Vicolo Osservatorio 5, I-35122 Padova, Italy*
[10]*Dipartimento di Fisica, Università Roma TRE, Viea della Vasca Navale, 84 00146, Roma, Italy*
[11]*Istituto do Radioastronomia, Via P. Gobetti 101, 40129, Bologna, Italy*
[12]*Cyprus College, 6 Diogenes Street, Engomi, P.O. Box 22006, 1516 Nicosia, Cyprus*
[13]*European Space and Technology Centre (ESTEC), Keplerlaan 1, 2201AZ Noordwijk, the Netherlands*
[14]*Institute of Astronomy, University of Cambridge, Madingley Road, Cambridge CB3 0HA*

ABSTRACT

We present the 90-μm luminosity function of the Final Analysis of the European Large Area *ISO* Survey (ELAIS), extending the sample size of our previous analysis (Paper IV) by about a factor of 4. Our sample extends to $z = 1.1$, ~ 50 times the comoving volume of Paper IV, and $10^{7.7} < h^{-2}L/\mathrm{L_\odot} < 10^{12.5}$. From our optical spectroscopy campaigns of the northern ELAIS 90-μm survey (7.4 deg² in total, to $S_{90\,\mu m} \geqslant 70$ mJy), we obtained redshifts for 61 per cent of the sample (151 redshifts) to $B < 21$ identified at 7 μm, 15 μm, 20 cm or with bright ($B < 18.5$) optical identifications. The selection function is well-defined, permitting the construction of the 90-μm luminosity function of the Final Analysis catalogue in the ELAIS northern fields, which is in excellent agreement with our Preliminary Analysis luminosity function in the ELAIS S1 field from Paper IV. The luminosity function is also in good agreement with the recent *IRAS*-based prediction of Serjeant and Harrison – which, if correct, requires luminosity evolution of $(1 + z)^{3.4 \pm 1.0}$ for consistency with the source counts. This implies an evolution in comoving-volume-averaged star formation rate at $z \lesssim 1$ consistent with that derived from rest-frame optical and ultraviolet surveys.

Key words: galaxies: evolution – galaxies: formation – galaxies: starburst – cosmology: observations – infrared: galaxies – submillimetre.

1 INTRODUCTION

Recent infrared surveys have revealed the existence of strongly evolving populations of far-infrared luminous galaxies. For exam-

⋆E-mail: s.serjeant@kent.ac.uk
†Visiting Astronomer, Observatorio Astrofísico Guillermo Haro, Cananea, Sonora, Mexico.

ple, the discovery of submillimetre luminous galaxies (Smail, Ivison & Blain 1997; Hughes et al. 1998) with median redshifts greater than two (Chapman et al. 2003) proves the existence of a radical change in the demographics of star formation. Luminous infrared galaxies ($\sim 10^{11}$ L$_\odot$) contributed at least as much to the comoving star formation rate at $z \sim 2$ as all optical/ultraviolet identified sources, but are negligible contributors locally. Furthermore, the spectrum of the extragalactic background (e.g. Puget et al. 1996;

Fixsen et al. 1998; Lagache et al. 1999) implies that approximately half the luminous energy emitted by stars throughout the history of the Universe was absorbed and re-emitted by dust in the far-infrared. Differences between the evolution of infrared luminous galaxies and that of galaxies selected in the rest-frame optical/UV may be in part attributable to the changes in the demographics of obscured versus unobscured star formation, but may also be related to large-scale structure density variations in the small-area surveys (e.g. ≪1 square degree) conducted to date (see discussion in Oliver et al. 2000). Consequently, while some of the most significant earlier contributions have been in small-area surveys (e.g. Hughes et al. 1998), the emphasis has since shifted to wide-area surveys (∼1–100 square degrees), which are less affected by cosmic variance problems (e.g. Oliver et al. 2000; Lonsdale et al. 2003).

The European Large Area *ISO* Survey (ELAIS) was the largest open-time survey on the Infrared Space Observatory (*ISO*), and resulted in the delivery of the largest catalogue of any survey on *ISO* (Rowan-Robinson et al. 2004) from both the ISOCAM instrument (Cesarsky et al. 1996) and ISOPHOT instrument (Lemke et al. 1996). The science goals are diverse, and discussed in detail in Oliver et al. (2000, hereinafter Paper I). Following the Preliminary Analysis of the ELAIS data (Efstathiou et al. 2000, hereinafter Paper III; Serjeant et al. 2000, hereinafter Paper II), a more exhaustive analysis of the data has been made resulting in deeper and better calibrated source lists (Lari et al. 2001; Gruppioni et al. 2002; Héraudeau et al. 2004, hereinafter Paper VIII), and is referred to as the ELAIS Final Analysis. The ELAIS survey complements the deeper surveys conducted by ISO (e.g. Franceschini et al. 2001 and references therein; Rodighiero et al. 2003) and the shallower ISOPHOT Serendipity Survey (Stickel et al. 2004).

The Final Analysis catalogue paper (Rowan-Robinson et al. 2004) presents the source list and redshifts obtained to date from ELAIS. These sources have been studied in earlier papers in this series. For example, Morel et al. (2001, hereinafter Paper VI) present the first hyperluminous galaxy discovered in ELAIS, several more of which are catalogued in the Rowan-Robinson et al. (2004) paper; Pozzi et al. (2003) compare the 15-μm, Hα and 1.4-GHz star formation rates of galaxies in the S2 field; Väisänen et al. (2002) report the near-infrared identifications of ELAIS galaxies, in the process obtaining a improved flux calibration that implies a modest correction to the Preliminary Analysis source counts (Serjeant et al. 2000) consistent with the Final Analysis source counts (Gruppioni et al. 2002); Basilakos et al. (2002, hereinafter Paper VII), Manners et al. (2003) and Manners et al. (in preparation) examine the X-ray properties of ELAIS galaxies. The evolution of AGNs in ELAIS is examined in Matute et al. (2002). The ELAIS fields have also been the subject of many subsequent multi-wavelength surveys (e.g. Ciliegi et al. 1999; Gruppioni et al. 1999; Alexander et al. 2001, hereinafter Paper V; Fox et al. 2002; Scott et al. 2002; Manners et al. 2003; Manners et al., in preparation) making the fields among the best studied degree-scale areas on the sky. Finally, the main ELAIS survey areas will shortly be observed by the SWIRE Legacy Survey (Lonsdale et al. 2003) on the *Spitzer Space Telescope*, making this catalogue extremely important for the rapid science exploitation of the *Spitzer* data.

The multiwavelength galaxy luminosity functions are one of the main observational constraints on the evolution of dust-enshrouded star formation in galaxy populations. In Serjeant et al. (2001, hereinafter Paper IV) we derived the 90-μm luminosity function of ELAIS galaxies in the Preliminary Analysis of the ELAIS S1 field (Efstathiou et al. 2000). We found good agreement with local determinations at the low-redshift end, and evidence for pure luminosity

evolution at the rate of $(1 + z)^{2.45 \pm 0.85}$. This is consistent with the optically-derived evolution in the comoving volume-averaged star formation rate (e.g. Glazebrook et al. 2003). In this paper we present the 90-μm luminosity function for the Final Analysis of the remaining areas (Héraudeau et al. 2004, hereinafter Paper VIII). Section 2 describes the sample selection and the data acquisition, and Section 3 presents the $1/V_{max}$ luminosity function. Section 4 discusses our results in the context of source count model evolution and the comoving star formation history.

We assume a Hubble constant of $H_0 = 100\,h = 72\,km\,s^{-1}\,Mpc^{-1}$, and a cosmology of $\Omega_M = 0.3$, $\Omega_\Lambda = 0.7$ throughout this paper. We adopt the convention of converting from 90-μm monochromatic luminosities to bolometric luminosities assuming $\nu L_\nu =$ constant, i.e. $10^{10}\,L_\odot$ corresponds to approximately $1.159 \times 10^{24}\,W\,Hz^{-1}$ at 90 μm. This choice simplifies the comparisons with other studies and does not affect the results in this paper.

2 METHOD

2.1 Sample selection

Our principal sample is the ELAIS 90-μm Final Analysis sample of Héraudeau et al. (2004) in the Northern ELAIS fields, covering a total of 7.4 square degrees to a flux limit of 70 mJy. The completeness as a function of flux is given in Héraudeau et al. (2004), and varies from ∼100 per cent at 150 mJy to ∼50 per cent at 70 mJy. The source counts at the faintest end (e.g. 70–130 μJy) differ from those of the Preliminary Analysis (Paper II, Paper IV). These data points were neglected in the fit to the source counts, from which the evolution rate was derived, so the evolution quoted in Paper IV is unaffected by the change in the catalogues at the faintest end. Notably, the source counts of the *optically identified* sources are identical in the Preliminary and Final Analyses. We do not have Final Analysis catalogues for the small ELAIS survey areas (Paper I), so we supplement the Final Analysis catalogue with optically identified sources from the Preliminary Analysis, which are almost entirely in these supplementary small fields. The exclusion of these sources does not affect the luminosity function determinations, apart from decreasing the spectroscopic sample size by seven objects. The catalogue has a total of 420 galaxies, of which we have optically identified 249 to magnitude limits discussed below. We have obtained optical spectroscopy of 151 of these optically identified galaxies to date.

Fig. 1 plots the luminosity–redshift plane for our sample. For the purposes of *K*-corrections, the rest-frame galaxy spectrum in the vicinity of 90 μm is assumed to follow $d\log L_\nu/d\log \nu = -2$, though this choice has very little affect on the derived luminosity function. There are no photometric redshifts used in the derivation of the luminosity function in this paper.

2.2 Data acquisition

ELAIS 90-μm galaxies were optically identified either purely from the Digitized Sky Survey (for which Paper IV found $B < 18.5$ is the limit for reliable identifications), or from the abundant multi-wavelength data from the ISOCAM mid-infrared ELAIS data (Paper II, Gruppioni et al. 2002) and/or the VLA follow-up mapping (Ciliegi et al. 1999). For the 90-μm galaxies identified with ISOCAM or the VLA, optical identifications brighter than $B < 21$ were sought using the Digitized Sky Survey and our own optical imaging (Rowan-Robinson et al. 2004). Given the astrometric errors of the multiwavelength identifications (∼1–3 arcsec) this
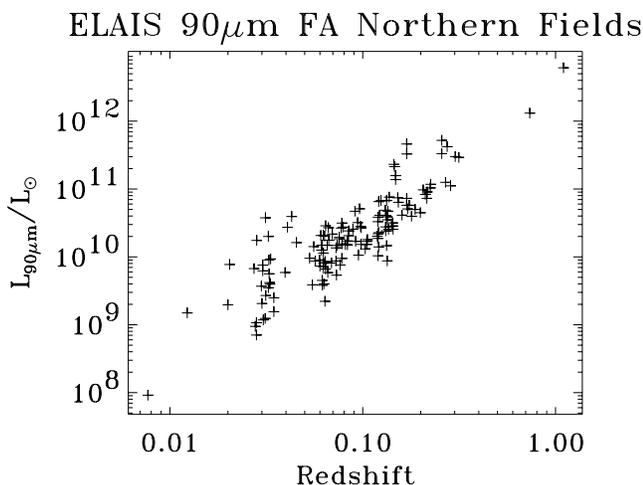
ELAIS 90μm FA Northern Fields

Figure 1. Luminosity–redshift plane for spectroscopically identified ELAIS 90-μm Final Analysis galaxies from the northern ELAIS fields. Monochromatic luminosities at 90 μm have been converted to bolometric luminosities assuming $\nu L_\nu =$ constant. No correction has been made for pure luminosity evolution.

magnitude limit is much more than sufficiently bright to ensure reliable optical identifications.

The optical identifications themselves are presented and discussed in Rowan-Robinson et al. (2004). It is possible that, despite the careful analysis in that paper, some of the identifications may be wrong; nevertheless, the almost-universal appearance of emission lines in our spectra (see below) implies that the overwhelming majority of the identifications *must* be correct. Even in cases where the identification is wrong, the spurious identification will often have the same redshift as the true identification because star-forming galaxies are well known to be more likely to have close companions than the field galaxy population as a whole (e.g. Surace, Sanders & Mazzarella 2004). Similarly, it is possible that at the ∼40 arcsec resolution of ISO, some point sources will in fact be blends of multiple sources. However, the ELAIS 90-μm survey is far from the point source confusion limit (e.g. Rowan-Robinson 2001), so any blends are likely to be physically associated galaxy pairs, such as interacting or merging systems. Again, this would not lead to incorrect redshift estimates for the purposes of the luminosity function. Also, in local galaxies there is little evidence that galaxies in pairs each contribute comparably to their total unresolved far-infrared flux (e.g. Surace et al. 2004). In summary, for the purposes of this paper we will assume that the identifications are all correct.

Spectroscopic campaigns were made on several runs at the William Herschel Telescope; the Guillermo-Haro 2.2-m Telescope, Cananea, Mexico; and the Kitt Peak WIYN facility. The Kitt Peak and William Herschel data are described in Perez-Fournon et al. (in preparation). The Guillermo-Haro data was taken on 2001 June 17–30, 2002 May 6–13 and 2002 July 1–10 using the LFOSC and Boller & Chivens low-dispersion spectrographs. Redshift errors are dominated by wavelength calibration accuracy (∼1–2 Å) and are negligible for the purposes of this paper. In total, we obtained spectroscopic redshifts of 61 per cent of the sample listed in Rowan-Robinson et al. (2004).

3 RESULTS

A luminosity function can be constructed for any sample *provided* that the selection function can be accurately stated, and that there are

no populations of objects that are undetectable at *any* redshift. For a single flux-limited sample, the number density in a given luminosity bin is given by

$$\Phi = \sum V_{\mathrm{max},i}^{-1} \tag{1}$$

with an associated rms error of

$$\Delta\Phi = \sqrt{\sum V_{\mathrm{max},i}^{-2}}, \tag{2}$$

where the sums are taken over the objects in the bin. The maximum volume V_{max} for each object is the comoving volume enclosed by the maximum redshift at which such an object is detectable, given the flux limit.

This procedure can easily be generalized for the presence of more complicated selection criteria, including the multiwavelength flux limits used in this paper. For example, if the selection function is a function of redshift, then this function must be used to weight the differential volume elements, which are then integrated to calculate a weighted V_{max} for each object. Paper IV (Serjeant et al. 2001) discusses in more detail the formalism for generating $1/V_{\mathrm{max}}$ luminosity functions in the presence of complicated selection functions. In this paper we largely restrict our discussion to the construction of the selection function, and refer the reader to Paper IV for its application to the luminosity function. The only modification of this approach of Serjeant et al. (2001) to this paper is in the consideration of bins containing only one galaxy. In this paper these bins (and only these bins) are treated as having a 1σ range of $(0.18 - 3.3)V_{\mathrm{max}}^{-1}$ (rather than $V_{\mathrm{max}}^{-1} \pm V_{\mathrm{max}}^{-1}$), corresponding to the $\pm 1\sigma$ likelihood limits of an underlying Poisson distribution with one detection (Gehrels 1986).

The optical completeness correction is the largest systematic uncertainty in our selection function. To estimate this, we plot in Fig. 2 the fraction of galaxies with spectroscopic redshifts, as a function of apparent magnitude. Note that this is a *differential* plot, i.e. at a magnitude m we only consider galaxies with magnitudes $m \pm 1$. We found that our luminosity function is robust to changes in the derivation of this optical completeness, such as considering galaxies with magnitudes $m \pm 1.5$ or $m \pm 2$ instead of $m \pm 1$, in that
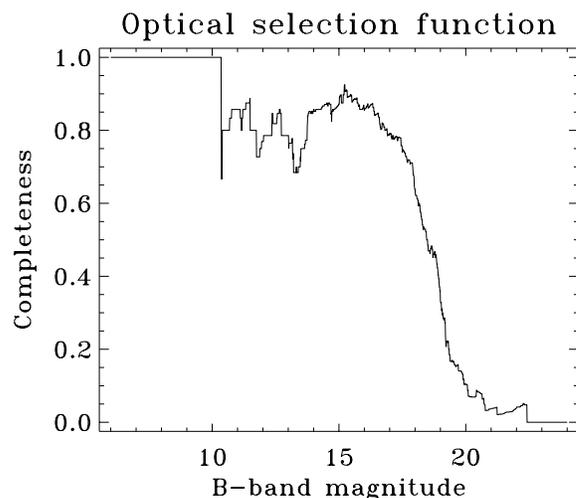
Optical selection function

Figure 2. Completeness of the optical spectroscopy, as a function of apparent B-band magnitude. At each magnitude m, the spectroscopic completeness plotted refers to galaxies with magnitudes in the interval $m - 1$ to $m + 1$. This curve has structure on scales smaller than ± 1 mag (e.g. discrete changes) as individual objects move in and out of the bin being considered.

any systematic changes to the derived luminosity function are very much smaller than the $\pm 1\sigma$ random errors.

To have an optical identification, each galaxy must either have a bright optical ID ($B < 18.5$) or be detected at 15, 7 µm or in the radio frequency range. In the case of 15-, 7-µm and radio frequency detections, the galaxy can be identified to fainter optical magnitudes ($B < 21$), since the greater astrometric accuracy of these catalogues makes reliable identifications possible to fainter magnitudes. The probability of a given galaxy having an identification is therefore given by

$$P_{ID} = 1 - (1 - p_{opt})(1 - p_{15\,\mu m})(1 - p_{7\,\mu m})(1 - p_{rad}). \qquad (3)$$

Here p_{opt} is the probability that this galaxy has a bright optical ID, and similarly for the 15-, 7-µm and radio frequency ranges. For a spectroscopically complete sample, p_{opt} is equal to one at red-shifts where the galaxy would have $B < 18.5$, and zero at higher redshifts. In our case, we use the optical completeness curve of Fig. 2 for the $B \leqslant 18.5$ range. Similarly, $p_{15\,\mu m}$ incorporates both the 15-µm completeness (e.g. Gruppioni et al. 2002) and the optical completeness from Fig. 2, i.e. $p_{15\,\mu m} = c_{15\,\mu m} \times c_{opt}$, where $c_{15\,\mu m}$ is the 15-µm completeness and c_{opt} is the completeness of optically-faint galaxies in the optical. Analogous optical completeness corrections were made for 7-µm and radio identifications. We calculate $P_{ID}(z)$ for every galaxy in our sample, and use it to weight the volume elements in the calculation of the total accessible volume V_{max} (Avni & Bahcall 1983) for each galaxy, following the procedure in Paper IV.

What is the best way of representing the luminosity function? One can make parametric fits, but these are subject to the assumptions in the parametrization; alternatively, one can directly bin the luminosity function, but this loses information. Dunlop & Peacock (1990) used a 'free-form' fitting technique in their analysis of the luminosity function of radio-loud active galaxies. In this methodology, a selection of high-order polynomials are fitted to the data. The arbitrariness and variation of the fitting functions partly avoids the issue of assumptions in the functional form. Divergence in the fits indicates lack of constraint, but unfortunately convergence does not necessarily imply constraint. Also, the range spanned by the models does not correspond to, for example, a $\pm 1\sigma$ constraint. In this paper we adopt an alternative approach, similar to that used in Serjeant et al. (2001): instead of binning the data into discrete bins, we calculate the luminosity function at *every* luminosity L in a bin of logarithmic width $\pm\delta \log_{10} L$. This has the advantage of returning a $\pm 1\sigma$ constraint at any luminosity, while explicitly controlling the balance between resolution (in luminosity) and loss of information with the choice of the boxcar size.

Fig. 3 shows the 90-µm$1/V_{max}$ luminosity function derived in this way. We compute the luminosity function in a logarithmic bin of width ± 0.5 dex. Fig. 3 also gives a comparison with the ELAIS Preliminary Analysis luminosity function from the ELAIS S1 field (Serjeant et al. 2001), and the agreement is excellent. However, a disadvantage of such a wide binning of the data is that there are effectively very few independent data points (e.g. four for a data set spanning four decades in luminosity). This was necessary for the small spectroscopic sample (37) in Paper IV, but the current sample of 151 is large enough to benefit from finer binning. Therefore in Fig. 4 we plot the 90-µm luminosity function for a ± 0.25-dex binning of the data. This figure also plots a comparison with the predicted 90-µm local luminosity function from the PSC-z survey (Serjeant & Harrison 2004), estimated from the *IRAS* colours of each of the 15411 PSC-z galaxies. In both Figs 3 and 4, the population is assumed to evolve with pure luminosity evolution at a rate
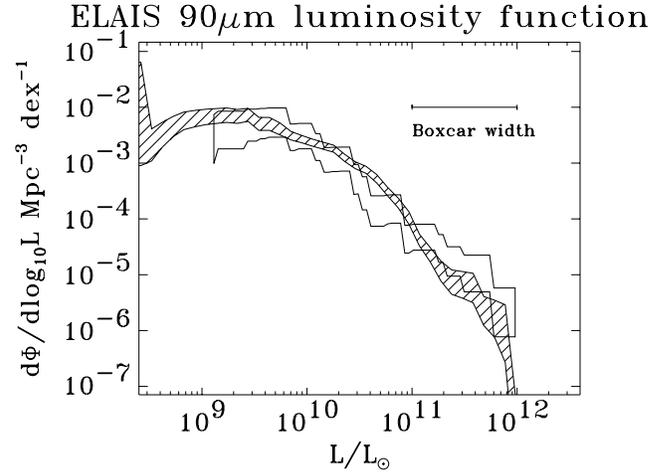

Figure 3. Shaded area shows the $\pm 1\sigma$ luminosity function constraint at 90 µm from the ELAIS Final Analysis of the northern ELAIS fields. Pure luminosity evolution of $(1 + z)^3$ is assumed, though this has only a small effect on the derived luminosity function except at the highest luminosities. Luminosities are converted to bolometric luminosities assuming $\nu L_\nu = $ constant. At each luminosity, the objects with luminosities ± 0.5 dex are used in the construction of the luminosity function, which is indicated on the diagram as the boxcar width. Also plotted as the unshaded bound area is the 90-µm ELAIS luminosity function from the Preliminary Analysis of the S1 field, which used the same boxcar width. Note the excellent agreement between the Preliminary and Final Analyses, and the much tighter constraint from the Final Analysis.
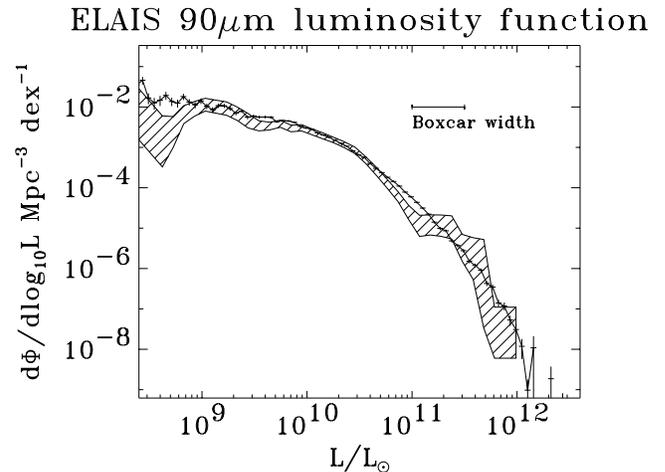

Figure 4. Shaded area shows the $\pm 1\sigma$ luminosity function at 90 µm from the ELAIS Final Analysis of the northern ELAIS fields, with a boxcar width of ± 0.25 dex (cf. Fig. 3). Pure luminosity evolution of $(1 + z)^3$ is assumed. Luminosities are converted to bolometric luminosities assuming $\nu L_\nu = $ constant. Also plotted is the predicted 90-µm local luminosity function from the PSC-z survey (Serjeant & Harrison 2004). Note the good agreement of the ELAIS luminosity function with this prediction.

of $(1 + z)^3$. This assumption does not affect the luminosity function determined from the data except at the brightest end (Fig. 1). The luminosity function is tabulated in Table 1.

4 DISCUSSION AND CONCLUSIONS

Using differential volume elements weighted to the selection function (Section 3), the $\langle V/V_{max} \rangle$ distributions hint at the existence of

Table 1. Tabulated luminosity function with boxcar width ± 0.25 dex, as plotted in Fig. 4.

Luminosity bin, $\log_{10}(L/L_{\odot})$	Φ (Mpc^{-3} dex^{-1})	$\Delta\Phi$ (Mpc^{-3} dex^{-1})
8.625 ± 0.25	1.86×10^{-3}	1.84×10^{-3}
8.75 ± 0.25	4.1×10^{-3}	2.62×10^{-3}
8.875 ± 0.25	8.4×10^{-3}	3.64×10^{-3}
$9. \pm 0.25$	1.14×10^{-2}	4.13×10^{-3}
9.125 ± 0.25	1.1×10^{-2}	3.89×10^{-3}
9.25 ± 0.25	9.38×10^{-3}	3.41×10^{-3}
9.375 ± 0.25	6.3×10^{-3}	2.35×10^{-3}
9.5 ± 0.25	4.07×10^{-3}	1.3×10^{-3}
9.625 ± 0.25	3.47×10^{-3}	7.84×10^{-4}
9.75 ± 0.25	3.88×10^{-3}	7.68×10^{-4}
9.875 ± 0.25	3.02×10^{-3}	5.57×10^{-4}
$10. \pm 0.25$	2.75×10^{-3}	4.73×10^{-4}
10.125 ± 0.25	2.06×10^{-3}	3.49×10^{-4}
10.25 ± 0.25	1.53×10^{-3}	2.38×10^{-4}
10.375 ± 0.25	1.09×10^{-3}	1.87×10^{-4}
10.5 ± 0.25	6.66×10^{-4}	1.24×10^{-4}
10.625 ± 0.25	3.16×10^{-4}	6.8×10^{-5}
10.75 ± 0.25	1.41×10^{-4}	3.45×10^{-5}
10.875 ± 0.25	5.85×10^{-5}	1.66×10^{-5}
$11. \pm 0.25$	2.14×10^{-5}	9.15×10^{-6}
11.125 ± 0.25	1.38×10^{-5}	7.27×10^{-6}
11.25 ± 0.25	1.38×10^{-5}	7.4×10^{-6}
11.375 ± 0.25	1.28×10^{-5}	7.39×10^{-6}
11.5 ± 0.25	3.98×10^{-6}	2.71×10^{-6}
11.625 ± 0.25	2.92×10^{-6}	2.61×10^{-6}
11.75 ± 0.25	1.54×10^{-7}	1.53×10^{-7}
11.875 ± 0.25	3.34×10^{-8}	$^{+7.68}_{-2.74} \times 10^{-8}$

90μm differential source counts

Figure 5. Source counts from ELAIS (filled circles, Héraudeau et al. 2004), the Lockman Hole (open circles Rodighiero et al. 2003), and local counts estimated from *IRAS* (crosses, Serjeant & Harrison 2004). Also overplotted are three model pure evolution curves of $(1 + z)^{\alpha}$, where $\alpha = 0$ (bottom curve, no evolution), $\alpha = 3$ (central curve) and $\alpha = 4$ (upper curve). All evolution is assumed to have stopped in these models at $z = 2$. Note the clear deviation of the source counts from the no-evolution case.

evolution in this population, but only at the $\sim 0.6\sigma$ level: assuming a no-evolution model yields $\langle V/V_{\max}\rangle = 0.523 \pm 0.029$, while assuming $(1 + z)^3$ pure luminosity evolution yields $\langle V/V_{\max}\rangle = 0.482 \pm 0.029$. With this test, deviation from $1/2$ is evidence for evolution (Avni & Bahcall 1983). However, this statistic is not the most efficient at detecting evolution.

Fig. 4 demonstrates that the ELAIS 90-µm luminosity function is consistent with the prediction from the local *IRAS* population by Serjeant & Harrison (2004). If we *assume* that this prediction is correct, then we can use the source counts to constrain the strength of the evolution. Fig. 5 plots the ELAIS 90-µm Final Analysis source counts (Héraudeau et al. 2004), together with the interpolated 90-µm *IRAS* counts from Serjeant & Harrison (2004). We also plot the predicted source counts for the predicted 90-µm luminosity function with $(1 + z)^{\alpha}$ pure luminosity evolution to $z = 2$, with $\alpha = 0, 3, 4$. Clearly, the source counts are a strong discriminant of the strength of the evolution. Provided the local luminosity function is of this form, the constraint on the evolution is $2.4 < \alpha < 4.4$ at 68 per cent confidence, or $1.3 < \alpha < 4.6$ at 95 per cent confidence. Is $z = 2$ the most appropriate redshift to halt the evolution? There is evidence that the evolution in the populations at 15 µm stops at $z \sim 1$ (Chary & Elbaz 2001; Franceschini et al. 2001; Xu et al. 2003). Decreasing the maximum redshift to which pure luminosity evolution extends from $z = 2$ to $z = 1$ slightly alters our constraints to $2.4 < \alpha < 4.6$ at 68 per cent confidence, or $1.3 < \alpha < 4.8$ at 95 per cent confidence. This evolution is consistent with that derived by us in Paper IV. Note that pure density evolution (PDE) can already be excluded as it overpredicts the sub-mJy radio source counts (Rowan-Robinson et al. 1993), and we do not consider PDE models further in this
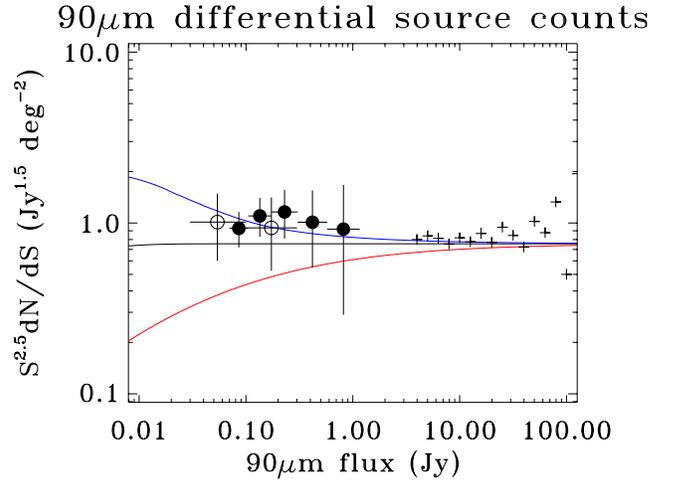
paper; however, it is worth noting that the far-infrared data alone is *not* sufficient to rule out pure density evolution.

This evolution rate is in good agreement with that derived from optically-selected galaxy samples (e.g. SLOAN, Glazebrook et al. 2003). Our data is consistent with the obscured star formation history and the corresponding unobscured history both evolving at similar rates, although the data at 90 µm also permits stronger evolution than that determined from the optically-selected samples. This is in agreement with the determinations from the sub-mJy radio population (e.g. Haarsma et al. 2000; Gruppioni, Oliver & Serjeant 2001), which are sensitive to both the obscured and unobscured high-mass star formation. However, the apparent plateau in the cosmic star formation history above $z = 2$ indicated by both optically-selected galaxies (e.g. Thompson 2003) and in the submillimetre range (e.g. Hughes et al. 1998; Fox et al. 2002; Scott et al. 2002) is difficult to reconcile with the current comoving mass density in stars, Ω_* (e.g. Blain et al. 1999; Serjeant & Harrison 2004). For the infrared luminous population, this may be in part due to contamination of the far-infrared flux by cirrus heating of the interstellar radiation field (Efstathiou & Rowan-Robinson 2003; Kaviani, Haehnelt & Kauffmann 2003). Alternatively, the initial mass function at high redshift may be skewed to high masses (e.g. Larson 1998; Franceschini et al. 2001; Serjeant & Harrison 2004).

The *Spitzer* satellite has already been successfully launched, and the prospects for improving on this analysis in the near future are excellent. The SWIRE survey (Lonsdale et al. 2003, 2004) will survey 70 square degrees including all the major ELAIS fields, deeper at 70 µm than the ELAIS survey at 90 µm. The source counts will be a powerful discriminant of the evolution, but more importantly the existence of large spectroscopic redshift surveys in the SWIRE fields (Rowan-Robinson et al. 2004) will be a powerful and immediate tool for the exploitation of this important legacy data set.

REFERENCES

Alexander D. et al., 2001, ApJ, 554, 18 (Paper V)
Avni Y., Bahcall J. N., 1983, ApJ, 235, 694
Basilakos S. et al., 2002, MNRAS, 331, 417 (Paper VII)
Blain A. W., Jameson A., Smail I., Longair M. S., Kneib J.-P., Ivison R. J., 1999, MNRAS, 309, 715
Cesarsky C. J. et al., 1996, A&A, 315, L32
Chapman S. C., Blain A. W., Ivison R. J., Smail I. R., 2003, Nat, 422, 695
Chary R., Elbaz D., 2001, ApJ, 556, 562
Ciliegi P. et al., 1999, MNRAS, 302, 222
Dunlop J. S., Peacock J. A., 1990, MNRAS, 247, 19
Efstathiou A., Rowan-Robinson M., 2003, MNRAS, 343, 322
Efstathiou A. et al., 2000, MNRAS, 319, 1169 (Paper III)
Fixsen D. J., Dwek E., Mather J. C., Bennett C. L., Shafer R. A., 1998, ApJ, 508, 123
Fox M. J. et al., 2002, MNRAS, 331, 839
Franceschini A., Aussel H., Cesarsky C. J., Elbz D., Fadda D., 2001, A&A, 378, 1
Gehrels N., 1986, ApJ, 303, 336
Glazebrook K. et al., 2003, ApJ, 587, 55
Gruppioni C. et al., 1999, MNRAS, 305, 297
Gruppioni C., Oliver S., Serjeant S., 2001, Ap&SS, 276, 791
Gruppioni C., Lari C., Pozzi F., Zamorani G., Franceschini A., Oliver S., Rowan-Robinson M., Serjeant S., 2002, MNRAS, 335, 831
Haarsma D. B., Partridge R. B., Windhorst R. A., Richards E. A., 2000, ApJ, 544, 641
Héraudeau Ph. et al., 2004, MNRAS, in press (doi:10.1111/j.1365-2966. 2004.08259.x) (Paper VIII)
Hughes D. H. et al., 1998, Nat, 394, 241
Kaviani A., Haehnelt M. G., Kauffmann G., 2003, MNRAS, 340, 739
Lagache G., Abergel A., Boulanger F., Désert F. X., Puget J.-L., 1999, A&A, 344, 322
Lari C. et al., 2001, MNRAS, 325, 1173
Larson R. B., 1998, MNRAS, 301, 569
Lemke D. et al., 1996, A&A, 315, L64
Lonsdale C. et al., 2003, PASP, 115, 897
Lonsdale C. et al., 2004, ApJS, 154, 54
Manners J. C. et al., 2003, MNRAS, 343, 293
Matute I. et al., 2002, MNRAS, 332, L11
Morel T. et al., 2001, MNRAS, 327, 1187 (Paper VI)
Oliver S. et al., 2000, MNRAS, 316, 749 (Paper I)
Pozzi F. et al., 2003, MNRAS, 343, 1348
Puget J.-L. et al., 1996, ApJ, 308, L5
Rodighiero G., Lari C., Franceschini A., Gregnanin A., Fadda D., 2003, MNRAS, 343, 1155
Rowan-Robinson M., 2001, ApJ, 549, 745
Rowan-Robinson M., Benn C. R., Lawrence A., McMahon R. G., Broadhurst T. J., 1993, MNRAS, 263, 123
Rowan-Robinson M. et al., 2004, MNRAS, 351, 1290
Scott S. et al., 2002, MNRAS, 331, 817
Serjeant S., Harrison D., 2004, MNRAS, submitted
Serjeant S. et al., 2000, MNRAS, 316, 768 (Paper II)
Serjeant S. et al., 2001, MNRAS, 322, 262 (Paper IV)
Smail I., Ivison R. J., Blain A. W., 1997, ApJ, 490, L5
Stickel M., Lemke D., Klass U., Krause O., Egner S., 2004, A&A, 414, 69
Surace J. A., Sanders D. B., Mazzarella J. M., 2004, AJ, 127, 3235
Thompson R. I., 2003, ApJ, 596, 748
Väisänen P. et al., 2002, MNRAS, 337, 1043
Xu C. K., Lonsdale C. J., Shupe D. L., Franceschini A., Martin C., Schiminovich D., 2003, ApJ, 587, 90

This paper has been typeset from a T_EX/L^AT_EX file prepared by the author.